Minimum Molecular Weight and Tie Molecule Content for Ductility in Polyethylenes of Varying Crystallinity

*Seong Hyuk Cho and Richard A. Register**

Department of Chemical and Biological Engineering, Princeton University, NJ 08544

TABLE OF CONTENTS GRAPHIC

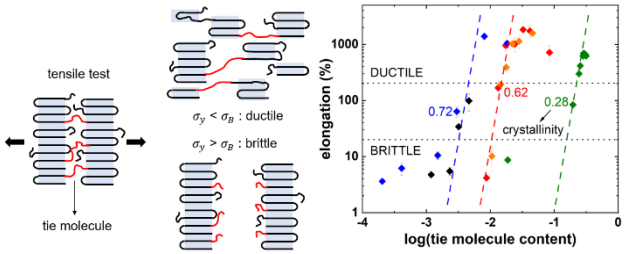

for Table of Contents use only

ABSTRACT

Semicrystalline polymers of low glass transition temperature, such as polyethylene (PE), can be either brittle or ductile depending on their content of intercrystallite stress transmitters—such as tie molecules (TMs), chains that directly bridge the intercrystalline amorphous layer. TM content will increase with increasing molecular weight (M), or with the fraction of high-M chains in a disperse polymer, and with decreasing intercrystallite repeat spacing d, which can be manipulated through thermal history and the incorporation of comonomer. The present work examines the failure mode of model narrow-distribution linear PEs (LPEs) of high crystallinity, where d is varied through crystallization history (either quenching or slowly cooling), and ethylene-butene copolymers (hydrogenated polybutadienes, hPBs) of moderate crystallinity, where d is limited by the short-branch content. For each series (LPEs with different thermal histories and quenched hPBs), a rather sharp brittle-to-ductile transition (BDT) is observed with increasing M, at a value M_{BDT}. However, across the three series, the value of M_{BDT} does not depend solely on the value of d; indeed, a higher M is required to achieve ductility in quenched samples of hPB than in LPE, despite the much lower values of d for hPB. Consequently, the calculated value of TM fraction at the BDT increases strongly as crystallinity decreases, by a factor of approximately 50 from slow-cooled LPE to quenched hPB. This strong dependence is explained by considering the influence of TMs on the brittle fracture stress (σ_b), with the BDT occurring when there are sufficient TMs for σ_b to exceed the yield stress (σ_y), which is strongly dependent on crystallinity but independent of TM content.

INTRODUCTION

In semicrystalline polymers, tie molecules (TMs) – chains that bridge two or more crystalline lamellae across the interlamellar amorphous layer – are widely recognized[1] as important determinants of mechanical behavior, including aspects such as yielding,[2,3] strain-hardening[3–6], and slow crack growth (SCG).[7–11] Bundles of TMs were directly observed by Keith et al.[12,13] more than half a century ago, in blends of polyethylene (PE) and paraffin wax from which the wax had been extracted. In the intervening decades, researchers have endeavored to quantify (vs. simply observe) TM content by a variety of indirect methods, such as measurements of brittle fracture stress at cryogenic temperatures,[14] infrared dichroism in strained specimens,[15] and the extent of swelling in solvent vapor,[16] but no direct experimental method has emerged. More commonly, TM content is modeled: calculated from experimentally-accessible quantities, such as a polymer's molecular weight distribution and the average crystallite and amorphous layer thicknesses. This approach was pioneered by Huang and Brown (HB),[8,9] by comparing the polymer coil size (radius of gyration R_g, or root-mean-square end-to-end distance R_0) to the critical distance (L_{crit}) which a tie molecule must span (scaling roughly with the intercrystallite repeat spacing d), as shown schematically in Figure 1. In such calculations, the coil size in the solid is taken to match that in the melt (the "solidification hypothesis",[17,18] confirmed by small-angle neutron scattering (SANS) experiments on PE[19–21] and isotactic polypropylene[22]). Thus, TM content can be increased either by: a) increasing the molecular weight (M) of the polymer (or more precisely, the fraction of chains of sufficiently high M to form a TM), or b) decreasing the intercrystalline spacing d, which can be achieved either by quenching or via copolymerization, as counits are typically excluded from crystals.[23] The copolymerization approach has been used to great advantage in the development of TM-rich bimodal PE grades with enhanced SCG resistance (and thus greatly extended lifetime

in pipe applications), wherein d is reduced by incorporating low levels of comonomer into the high-M component.[24–26] Subsequent refinements of the HB approach have incorporated additional microstructural features,[6,27,28] but the central idea remains: the relative magnitudes of the polymer coil size and the intercrystalline distance are the principal determinants of TM content.

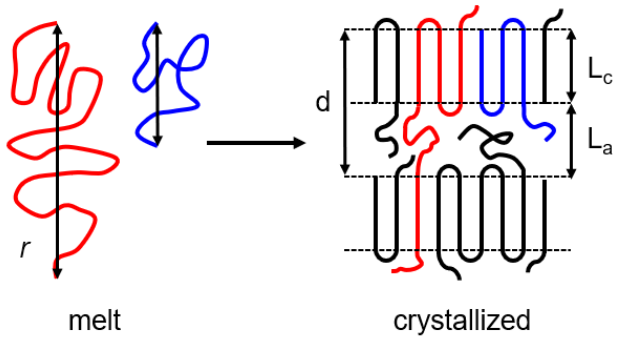

Figure 1. Schematic representation of the Huang-Brown idea. If the end-to-end distance of a coil r is sufficiently large (red) that portions of the same chain can form stems embedded in different crystallites, then that chain can form a TM upon solidification, whereas chains that are too short (blue) cannot. The average intercrystallite repeat distance d is also illustrated; in the simple two-phase model, d is the sum of the crystal thickness (L_c) and the amorphous layer thickness (L_a).

Though the post-yield and SCG behaviors of PE have been the subjects of extensive study in recent decades, the question of whether a polymer will be brittle or ductile in a simple stress-strain test is simultaneously both older and less-studied. Even well before the work of Huang and Brown, M was recognized as a key parameter in promoting ductility, and several early studies[29–33] on fractions of linear PE (LPE, devoid of comonomer or branching) found a brittle-to-ductile transition (BDT) in room-temperature tensile tests as M was increased. Values of M at the BDT (M_{BDT}) derived from published data on narrow-distribution LPE fractions vary somewhat, even in quenched or molded samples, from <30 kg/mol[31] to >40 kg/mol;[34] moreover, M_{BDT} increases when

the polymers are crystallized at shallower undercoolings.[34] One might hypothesize that a critical TM content is required for a polymer to show ductility; in this case, the variability in M_{BDT} in these studies, and the observed increase in M_{BDT} at shallower undercoolings, could simply reflect variations in *d*, through variations in thermal history.

The aim of the present work is to test this hypothesis, with the broader goal of elucidating the qualities and microstructural features required for room-temperature ductility. A range of narrow-distribution model PEs is investigated, especially LPEs obtained by hydrogenation of polycyclopentene (PCP, synthesized by ring-opening metathesis polymerization, ROMP), and binary blends of these LPEs. These high-crystallinity LPEs are supplemented by data for lower-crystallinity model ethylene-butene copolymers, obtained by hydrogenation of low-vinyl polybutadiene (synthesized by anionic polymerization), denoted hPB here. TM content is calculated via the HB approach. We find that while reducing *d* indeed favors ductility, the BDT does not in fact occur at a particular value of TM content across the range of materials, and that the TM content at the BDT increases strongly as the crystallinity decreases. This unanticipated result is explained by consideration of how TMs separately impact the brittle fracture stress and the yield stress.

EXPERIMENTAL PROCEDURE

Materials. For ROMP, cyclopentene (CP) monomer (Sigma-Aldrich, 96%) was distilled through a 71 cm Hempel column filled with 8 mm ceramic Berl saddles to reduce the 1-pentene level to < 5 ppm (undetectable by ^{1}H NMR) and thereby suppress acyclic chain transfer.[35] The distilled fractions were subjected to freeze-pump-thaw cycles to remove oxygen and dried over *s*-butyllithium and 1,1-diphenylethylene until the red adduct formed; cyclopentene was then vacuum transferred into a storage flask. The Mo-based Schrock initiator, 2,6-

diisopropylphenylimidoneophylidenemolybdenum(VI) bis(*t*-butoxide), was purchased from Strem Chemicals and used as received. Trimethylphosphine, PMe_3 (Sigma-Aldrich, 97%), was stirred overnight with sodium to remove water, degassed via freeze-pump-thaw cycles, and vacuum transferred. Propionaldehyde (Sigma-Aldrich, 97%) was stirred over 3 Å molecular sieves to remove water and degassed via freeze-pump-thaw cycles. Toluene (solvent for ROMP) was passed through an MBraun solvent purification system connected to the glovebox. For anionic polymerization, butadiene was collected and purified as previously described.[36] The solvent for anionic polymerization, mixed hexanes (>98.5%), was dried over *t*-butyllithium (Sigma Aldrich, 1.7 M in pentane) and 1,1-diphenylethylene until the red adduct formed, and degassed by freeze-pump-thaw cycles. For hydrogenation, palladium supported on calcium carbonate ($Pd/CaCO_3$, 5 wt% Pd) was purchased from Alfa Aesar, while H_2 (99.999%) was purchased from Airgas; both were used as received.

Polymerizations. All degassed and dried ROMP reagents were moved into an MBraun UNIlab glovebox with an N_2 atmosphere (O_2, H_2O < 0.1 ppm). ROMPs were performed in round bottom flasks with magnetic stirring. The Schrock initiator was first dissolved in toluene in a scintillation vial and transferred into the flask. PMe_3 and CP were added sequentially such that the initial CP concentration was 10 mol/L. A CP/Mo ratio of 5000:1 was used except for the synthesis of the PCPs of highest and second-highest molecular weight, where CP/Mo = 25000 and 7500 were used, respectively. PMe_3 was added to slow propagation relative to initiation and thereby decrease the dispersity of resulting polymer;[35,37] the PMe_3/Mo ratio was 15:1. Each ROMP was terminated at a specific time, corresponding to a specific CP conversion (8-16%), to achieve a targeted value of M_n, according to a previously-developed kinetic model.[35] The terminating agent was propionaldehyde, added in 50-fold excess to the initiator. After polymerization, PCP was

precipitated into methanol and dried under vacuum overnight. The detailed procedure employed for anionic polymerization of butadiene has been described previously;[36] polymerizations were conducted at 60 °C in mixed hexanes, initiated by *t*-butyllithium, yielding polybutadienes (PBs) with approximately 8% 1,2-addition.[36,38,39]

Hydrogenation. Catalytic hydrogenation was conducted over $Pd/CaCO_3$. Each polymer was dissolved (PCP in *n*-heptane, PB in cyclohexane) at 5 g/L with 0.5 wt% of butylated hydroxytoluene (BHT) relative to polymer to prevent oxidative degradation. The polymer solution was transferred to a 2 L Parr stainless steel reactor and $Pd/CaCO_3$ was added at a 2:1 weight ratio of catalyst (including support) to polymer. The reactor was charged with 400 psi of H_2 at room temperature and stirred at 130 °C for PCP or 100 °C for PB for 24 h, by which point saturation had reached >99.9% for PCP by determined by ^{1}H NMR spectroscopy[40] and >99% for PB determined by FTIR spectroscopy.[36] The hydrogenated polymers were recovered by hot filtration, precipitated into methanol, and dried under vacuum overnight. Previous studies have repeatedly shown that hydrogenation over $Pd/CaCO_3$ under these conditions is not accompanied by chain rearrangements.[38,40–43]

Molecular characterization. Molecular weights of the PCPs were determined by gel permeation chromatography (GPC) with tetrahydrofuran (THF) as the mobile phase (1 mL/min), employing two 30 cm Agilent PLgel Mixed-C columns, and Wyatt Optilab T-rEX differential refractive index (DRI; 25 °C, 658 nm wavelength) and miniDAWN TREOS three-angle light scattering (ambient temperature, 658 nm) detectors. Dispersities (Đ) were determined from the DRI elution time trace calibrated against narrow-distribution polystyrene (PS) standards, and the true molecular weight distribution curves were obtained by correcting[44] the DRI output for the difference in hydrodynamic volume between PS and PCP or PB at a common *M* (hydrodynamic

equivalence ratio r_{PB}[44] = 1.96, r_{PCP}[35] = 2.11). Weight-average molecular weight (M_w) values were determined from the light scattering results, using a specific refractive index increment dn/dc = 0.1212 mL/g for PCP[35] and 0.1251 mL/g for PB,[36] both in THF, at 25 °C and 658 nm. Values of the number-average molecular weight M_n were obtained as $M_n = M_w/Đ$.

Solution blending. Bimodal LPE blends were prepared from the LPEs having M_n = 27 and 78 kg/mol, by solution blending in xylene. The content of 78 kg/mol LPE was varied from 5 wt% to 80 wt%. To prevent oxidative degradation, xylene was first degassed by boiling, cooled to room temperature, and 1 wt% of BHT (relative to solvent) was added. The necessary masses of the component LPEs were added to degassed xylene to make a solution containing 3 wt% total polymer. The xylene was heated to boiling with vigorous stirring until the LPEs were completely dissolved, according to thorough visual inspection; the solution was then poured into -20 °C methanol, causing near-instantaneous crystallization with no indication of polymer in the supernatant. Precipitated blends were recovered by filtration and dried under vacuum at 70 °C overnight to remove any residual solvent. ^{1}H NMR confirmed complete removal of BHT from the polymer.

Crystallization. Polymers were crystallized by melt-pressing specimens between poly(ethylene terephthalate) sheets (0.254 mm thick) at 160 °C to make approximately 0.3 mm films, and either quenching (Q) into room temperature water or slowly cooling (SC) in the press. These thermal treatments correspond to cooling at approximately 1000 °C/min (Q) or 1 °C/min (SC) through the freezing point of PE as measured previously.[45]

Tensile testing. Room-temperature uniaxial stress-strain tensile testing was performed using an Instron 5865. Specimens were stamped out with an ASTM D1708 die (dogbone-shaped, 2.22 cm gauge length) from the compression-molded sheets. Specimens were extended at a

constant crosshead speed of 2.54 cm/min (initial strain rate = 0.87 min^{-1}) until break. The deformation rate is known to weakly influence the BDT in LPE, with order-of-magnitude reductions in the strain rate favoring ductility;[46] consequently, all specimens were tested with a common strain rate history. Three specimens were tested to obtain an average and standard deviation of the yield stress (σ_y, engineering stress; force at yield divided by initial cross-sectional area) and apparent overall breaking strain (ε_b, crosshead displacement at break divided by initial gauge length) except for a few materials that were too brittle to successfully prepare multiple dogbone samples.

Small-angle x-ray scattering (SAXS). SAXS measurements were conducted using an Anton-Paar compact Kratky camera. CuKα radiation (wavelength λ = 0.15418 nm) was produced by a PANalytical PW3830 generator with a long-fine-focus Cu tube, and an MBraun OED-50 M position sensitive detector was used to obtain the scattering profile. Rectangular specimens were cut from the same compression-molded sheets used for tensile testing. Data were corrected for detector linearity and sensitivity, empty beam scattering, sample thickness, and transmittance and desmeared for slit length using the iterative method of Lake.[47] Scattered intensity was calibrated to absolute units (I/I_eV) using a polyethylene standard,[48] and plotted against the magnitude of the momentum transfer vector $q = (4\pi/\lambda)\sin\theta$, where θ is half the scattering angle. The long spacing, d, was determined as $d = 2\pi/q^*$, where q^* is the primary peak position in a plot of $q^2(I/I_eV)$ vs q; the q^2 factor approximately corrects for the form factor of lamellae.[49]

Differential scanning calorimetry (DSC). DSC was conducted on specimens punched from the same compression-molded sheets employed for tensile testing, on a PerkinElmer DSC 7 equipped with a Type II intracooler and calibrated with indium and mercury standards. Thermograms were collected during the initial heating at 10 °C/min to preserve the samples'

crystallization history (SC vs Q). Weight fraction crystallinities were determined by dividing the measured melting enthalpy by 290 J/g,[50] corresponding to the melting enthalpy of 100% crystalline PE. These values were converted to room-temperature volume fraction crystallinities ϕ_c using crystalline[51] and amorphous phase[52] densities of $\rho_c = 1.000$ g/cm^3 and $\rho_a = 0.855$ g/cm^3.

RESULTS AND DISCUSSION

Table 1 summarizes essential quantities for the PEs examined in this work, including both molecular parameters (M_n and Đ), and characteristics (volume fraction crystallinity ϕ_c; breaking strain ε_b; etc.) which depend on specimen crystallization history: here, either quenched (Q) or slow-cooled (SC). Individual LPE and hPB polymers are coded by their M_n value; molecular weight distribution curves are provided in the Supporting Information (Figures S1 and S2). Binary LPE blends, prepared from LPE27K and LPE78K, are coded by the weight fraction of the high-M component (e.g., B15 contains 15 wt% PE78K); M_n and Đ values for the bimodal blends were calculated from the values for the two constituents and the blend ratio. Data collected for this work on two hPBs (hPB49K and hPB82K) were supplemented by drawing from the extensive work of Crist et al.[53,54] on hPBs of varying M_n, synthesized similarly. hPBs are model linear low-density polyethylenes (ethylene-butene copolymers[55]) with approximately 20 ethyl branches per 1000 backbone carbons, with significantly lower intercrystallite repeat spacings and degrees of crystallinity than the model LPEs synthesized by ROMP. Only quenched specimens of the hPBs were examined; thermal history is known[54] to have a much weaker effect on ϕ_c and especially on d in hPB than in LPE.

Table 1. Selected molecular, mechanical, and morphological parameters for PEs examined in this work.

Thermal History	Polymer	M_n (g/mol)	Đ	ε_b (%)[b]	σ_y (MPa)	ϕ_c	$2L_c+L_a$ (nm)	$\log_{10}(P_{2Lc+La})$
Q	LPE27K	26700	1.09	4[c]	-	0.64	33.2	-2.06
	LPE31K[a]	31200	1.08	170 ± 50	26.1	0.62	33.9	-1.88
	LPE37K	37400	1.12	960 ± 190	25.5	0.59	35.7	-1.76
	LPE43K	43300	1.15	1020 ± 290	25.6	0.59	37.1	-1.62
	LPE54K	53600	1.18	1840 ± 50	23.5	0.55	38.7	-1.49
	LPE78K	77700	1.16	1740 ± 410	20.6	0.53	43.6	-1.38
	LPE135K	135000	1.21	720 ± 220	20.3	0.47	47.4	-1.07
SC	LPE27K	26700	1.09	-[d]	-	0.82	55.1	-4.41
	LPE31K	31200	1.08	4[c]	-	0.78	52.6	-3.69
	LPE37K	37400	1.12	6 ± 2	-	0.74	55.7	-3.39
	LPE43K	43300	1.15	10 ± 2	-	0.72	54.4	-2.82
	LPE54K[a]	53600	1.18	60 ± 10	30.3	0.70	56.4	-2.52
	LPE78K	77700	1.16	1400 ± 160	29.4	0.70	58.7	-2.09
	LPE135K	135000	1.21	1040 ± 10	28.0	0.67	69.3	-1.74
Q	B5	27600	1.16	10 ± 5	-	0.64	33.1	-1.98
	B15[a]	29600	1.29	190 ± 20	24.3	0.61	33.0	-1.83
	B25	31900	1.39	390 ± 50	23.2	0.60	33.5	-1.75
	B40	36200	1.48	1020 ± 170	24.2	0.60	34.7	-1.65
	B60	44000	1.49	1140 ± 310	23.3	0.57	37.1	-1.55
	B80	56200	1.39	1590 ± 80	19.5	0.53	37.0	-1.34
SC	B25	31900	1.39	5[c]	-	0.78	55.8	-2.92
	B40	36200	1.48	6 ±1	-	0.76	55.1	-2.63
	B60[a]	44000	1.49	30 ±3	30.6	0.73	57.4	-2.49
	B80[a]	56200	1.39	100 ± 30	30.4	0.72	58.8	-2.33

	hPB13K[e]	12600	1.05	9	-	0.41	19.7	-1.73
	hPB42K[a,e]	41500	1.05	80	5.8	0.28	18.0	-0.71
	hPB49K	49000	1.07	420 ± 40	4.7	0.24	15.2	-0.59
	hPB58K[e]	57800	1.05	300	4.5	0.24	17.3	-0.61
Q	hPB82K	82100	1.12	690 ± 10	4.4	0.24	16.0	-0.54
	hPB91K[e]	91000	1.05	620	4.5	0.24	17.3	-0.55
	hPB118K[e]	118000	1.05	680	3.8	0.21	17.0	-0.53
	hPB143K[e]	143000	1.05	660	4.5	0.21	17.0	-0.51
	hPB189K[e]	189000	1.05	620	3.9	0.21	16.9	-0.50

[a]Polymers that fail in "transition" mode.

[b]Average ± standard deviation.

[c]Only one specimen was successfully tested due to extreme brittleness.

[d]Polymer was too brittle to stamp out any dogbone specimen without fracture.

[e]Data from Crist et al.[53,54]

Brittle-to-ductile transition with increasing *M*. The room-temperature failure mode of each LPE specimen was categorized as either brittle, ductile, or transition,[34] as represented by the stress-strain curves for three LPEs in Figure 2. Brittle failure is characterized by sample fracture prior to reaching a yield point ($\varepsilon_b < 20\%$), while ductile samples develop a stable neck across the entire specimen and draw, achieving $\varepsilon_b > 200\%$. Samples in the transition region[14] are characterized by the formation of an unstable neck followed by tearing, with an apparent specimen $\varepsilon_b = 20 - 200\%$ measured by the Instron crosshead displacement. Post-failure photographs of representative LPE specimens are provided in the Supporting Information (Figure S3), along with

all stress-strain curves (Figures S4-S17). The same ranges of ε_b were applied to categorize the failure mode of the hPBs.

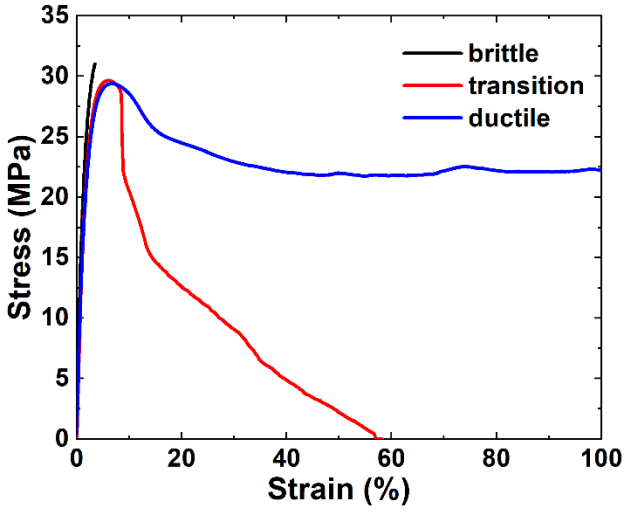

Figure 2. Representative stress-strain curves illustrating the brittle (LPE31K, SC), transition (LPE54K, SC), and ductile (LPE78K, SC) failure modes.

Table 1 lists the breaking strains (ε_b) for the various specimens, along with the yield stress (σ_y) for the specimens in the transition and ductile regimes. For each chemistry (LPE vs hPB) and thermal history (SC vs Q, for LPE), there is a narrow range of M_n over which the transition between brittle and ductile failure occurs; these transitions are centered near M_{BDT} = 60 kg/mol (LPE, SC), 30 kg/mol (LPE, Q), and 45 kg/mol (hPB, Q). The binary LPE blends exhibit the BDT at very similar values of M_n to the individual LPEs, suggesting that the breadth of the molecular weight distribution does not play a strong role (at fixed M_n), at least for the modest breadths examined here. LPE27K is brittle for either thermal history; blending LPE78K into LPE27K can thus impart ductility, although a much larger content of LPE78K is required to achieve ductility in SC blends (>80 wt% LPE78K) than in Q blends (≈20 wt%). The larger value of M_{BDT} for SC vs Q specimens of LPE (or equivalently, the higher weight fraction of LPE78K in the SC vs Q blends at the BDT)

is qualitatively consistent with the Huang-Brown idea, as SC specimens will have larger values of d. However, the significantly larger value of M_{BDT} for hPB vs LPE (Q specimens) is unanticipated, as the hPBs are expected to have significantly smaller values[54] of d, but very similar values[56] of melt R_0 at given M. This motivated a deeper study of the morphology of these specimens, for a quantitative comparison of the failure mode with respect to calculated tie molecule content across the series.

Solid-state morphology. The volume fraction crystallinities ϕ_c for the LPEs and blends (both thermal histories), and the two hPBs synthesized in-house, were determined from the DSC melting enthalpy. Crist et al.[54] reported densities rather than melting enthalpies for their hPBs; an adjustment was made to values of the fractional crystallinity derived from density to place them on the same footing as ϕ_c derived from DSC (see Supporting Information). The intercrystalline spacing d was measured by SAXS (SAXS patterns for all materials are presented in the Supporting Information, Figures S18-S22), and the crystalline and amorphous layer thicknesses were calculated according to the simple two-phase model as $L_c = \phi_c d$ and $L_a = (1-\phi_c)d$ (values of d, L_a, and L_c are listed in the Supporting Information, Tables S1-S3).

For hPB, d is largely set by the ethyl branch content; M_n and thermal history have little influence[54] on d. On the other hand, both M_n and thermal history have a substantial effect on d for LPE, as shown in Figure 3a; d increases monotonically with M_n for both thermal histories (Q and SC), at a similar rate, with a difference between Q and SC specimens of approximately 9 nm. This is consistent with the observations made by Robelin-Souffaché and Rault[57,58] on narrow-distribution LPE fractions, where d was found to scale roughly with $\sqrt{M_n}$ (see Figure S23 for a plot of d vs $\sqrt{M_n}$). Figure 3c shows that ϕ_c drops with increasing M_n, also as observed

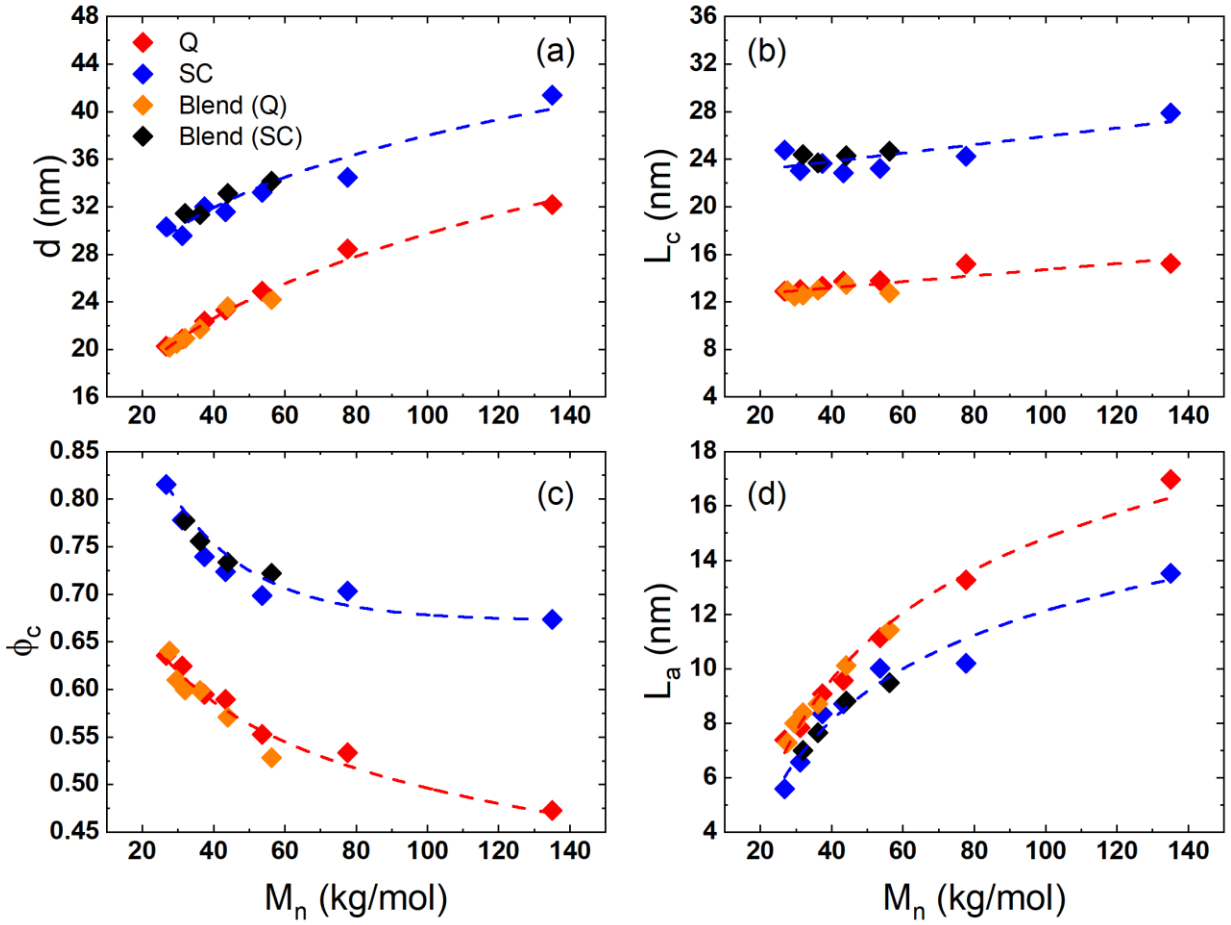

Figure 3. Plots of (a) long spacing d, (b) crystal thickness L_c, (c) volume fraction crystallinity (ϕ_c), and (d) amorphous layer thickness L_a of the individual LPEs and bimodal LPE blends crystallized from the 160 °C melt by either quenching (Q) or slow cooling (SC). Dashed lines are guides to the eye.

previously,[34,57] reaching values of 0.67 and 0.47 for SC and Q samples of LPE135K, respectively. Figures 3b and 3d together show that, for both thermal histories, the increase in d with M_n primarily reflects dilation of the amorphous layer; for each thermal history, L_c remains within a band of ±10% over the range of M_n examined, while L_a increases by 130% for the Q series, and 240% for

the SC series, as M_n is increased from 27 to 135 kg/mol. At a fixed M_n, SC samples have substantially larger L_c values (by 10 nm on average) compared to Q samples, while L_a values for SC samples are slightly smaller than for Q samples (by approximately 2 nm). The difference in L_c between Q and SC samples, and the relative constancy of L_c for a given crystallization history, are as expected from theory, where the degree of undercooling sets the crystal thickness.[59,60] Figure 3 shows that all the solid-state quantities (d and ϕ_c, and therefore L_c and L_a) are quite similar between the individual narrow-distribution LPEs and the bimodal blends, at the same M_n; hence d and ϕ_c are primarily affected by thermal history and M_n and not significantly by Đ, at least at the modest dispersities characteristic of these blends (<1.5).

TM fraction calculation. The HB model is employed to calculate the probability P that a polymer chain's end-to-end distance (r) in the melt is greater than the critical distance (L_{crit}) which a chain must span to form a tie between two crystalline lamellae.[8,9] For a monodisperse polymer, the HB model is given by Equations (1) – (3):

$$P = \frac{1}{3}\frac{\int_{L_{crit}}^{\infty} r^2 \exp(-b^2 r^2) dr}{\int_0^{\infty} r^2 \exp(-b^2 r^2) dr} \quad \text{Equation (1)}$$

$$b^2 = \frac{3}{2R_0^2} \quad \text{Equation (2)}$$

$$R_0^2 = KM \quad \text{Equation (3)}$$

where P is the fraction of polymer chains which form ties and K is a constant reflecting the chain stiffness. For LPE,[19,56] K = 1.25 Å^2-mol/g (1.21 Å^2-mol/g for hPB[56]), which translates to a characteristic ratio C_∞ = 7.4, slightly larger than the value of 6.8 used originally by Huang and Brown.[8,9] The prefactor 1/3 accounts for the fact that the lateral dimensions of the lamellae are

typically orders of magnitude greater than the interlamellar distance.[8,9] For polydisperse polymers, Equation (1) is integrated over the molecular weight distribution, yielding:

$$P_{avg} = \frac{\int_0^\infty nP(M)dM}{\int_0^\infty ndM} \qquad \text{Equation (4)}$$

where P_{avg} is the (number) fraction of chains which form TMs, $P(M)$ is P calculated from Equation (1) at each value of M across the molecular weight distribution, and n is the mole fraction of chains having molecular weight M. To apply Equation (1), a value of the critical distance L_{crit} must be selected; here, following the later work of Huang and Brown,[9] we chose $L_{crit} = 2L_c + L_a$. While other choices for L_{crit} have been proposed (e.g., $L_{crit} = 2L_c + 2L_a = 2d$ in reference 8, or $L_{crit} = \sqrt{6}d$ in reference 61)—and the choice of L_{crit} (like the prefactor of 1/3) certainly affects the absolute magnitude of P_{avg}—it does not substantially influence any of the comparisons made in this work. (See the Supporting Information, Figure S24, for results with $L_{crit} = 2L_c + 2L_a$, and Figure S25, where the correlating parameter is simply R_0/d, rather than P.) Similarly, bridging entanglements—formed by interlocking loops emanating from adjacent crystallites—are also effective stress transmitters and should favor ductility.[16] While such interlocking loops are undoubtedly present,[16,62] their content must scale comparably to that of tie chains (increasing with M, decreasing with d), and thus the straightforward HB calculation of TMs should be sufficient to rank and compare the content of stress transmitters across the series of PEs we examine here.

For each individual LPE and the two hPBs synthesized in-house, P_{avg} was calculated according to Equation (4), using the experimentally-measured molecular weight distributions (Figures S1 and S2); this value of P_{avg} is denoted as P_{2Lc+La} henceforth, to indicate the specific choice of L_{crit}. Values of $2L_c + L_a$ are given for each polymer and thermal history in Table 1, along

with calculated values of $\log_{10}(P_{2Lc+La})$. For the bimodal LPE blends, P_{2Lc+La} was calculated following Equation (5):

$$(P_{2Lc+La})_{blend} = n_1(P_{2Lc+La})_1 + n_2(P_{2Lc+La})_2 \qquad \text{Equation (5)}$$

where n_1 and n_2 are the mole fractions of LPE27K and LPE78K, respectively, and the values of $(P_{2Lc+La})_i$ are calculated using the value of $2L_c + L_a$ appropriate to the blend. For the hPBs studied by Crist et al.,[53,54] values of P_{2Lc+La} were calculated by Equation (1), considering the polymer to be monodisperse at its M_n value. Since P_{2Lc+La} is a number-fraction quantity, the modest distribution of chain lengths present in these anionically-synthesized polymers has a negligible influence on the calculated value of P_{2Lc+La} at a given M_n.

Figure 4 shows the variation in $2L_c + L_a$ and in P_{2Lc+La} with M_n, for the LPEs and bimodal blends with both thermal histories. $2L_c + L_a$ is approximately 19 nm smaller in Q vs SC samples, leading to a dramatic increase in P_{2Lc+La}, which is 5× higher in Q vs SC specimens at the highest M_n, with the factor increasing as M_n is reduced. While $2L_c + L_a$ increases slowly with M_n within each series (Q and SC), this has a relatively minor effect on the calculated values of P_{2Lc+La}. For the hPBs, $2L_c + L_a$ is essentially invariant with M_n (Table 1).

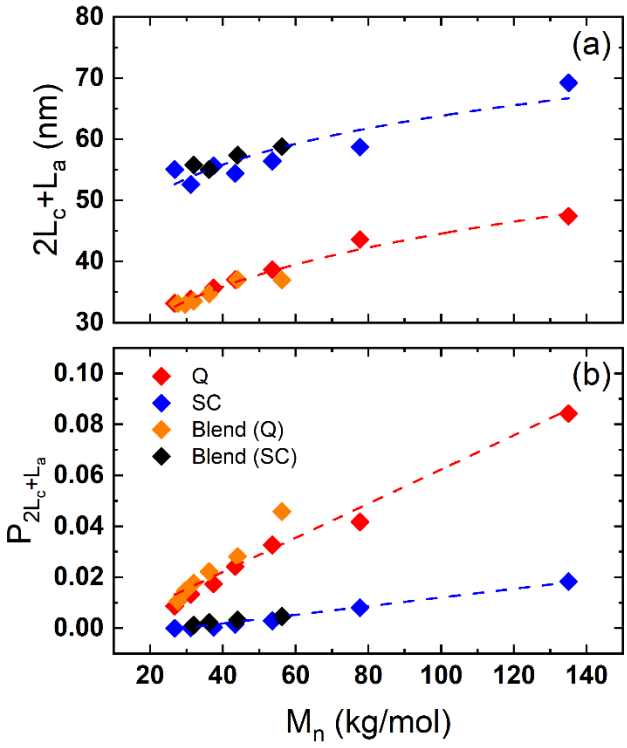

Figure 4. Plots of (a) $2L_c + L_a$ and (b) P_{2Lc+La} of individual LPEs and bimodal LPE blends with different thermal histories (Q and SC) vs M_n. Note the much higher value of P_{2Lc+La} for Q specimens, due to the lower d achieved by quenching. Dashed lines are guides to the eye.

The breaking strain (ε_b) values of all materials are plotted against $\log_{10}(P_{2Lc+La})$ in Figure 5. Notably, for a given thermal history (Q vs SC), the blend and individual LPE data superimpose well. Also notable is that the hPB data collected in this work agree well with those from Crist et al.[53,54] But contrary to expectations, the data do not even approximately collapse onto a single curve of ε_b vs P. Rather, they divide into three clear groups: LPE(SC), LPE(Q), and hPB, each with a very different threshold tie molecule content at the BDT. Numerically, the differences in this threshold value (P_{BDT}) amongst the three series are strikingly large (note the logarithmic abscissa in Figure 5): a factor of ≈3 between LPE(SC) and LPE(Q), and a further factor of ≈15 between LPE(Q) and hPB(Q).

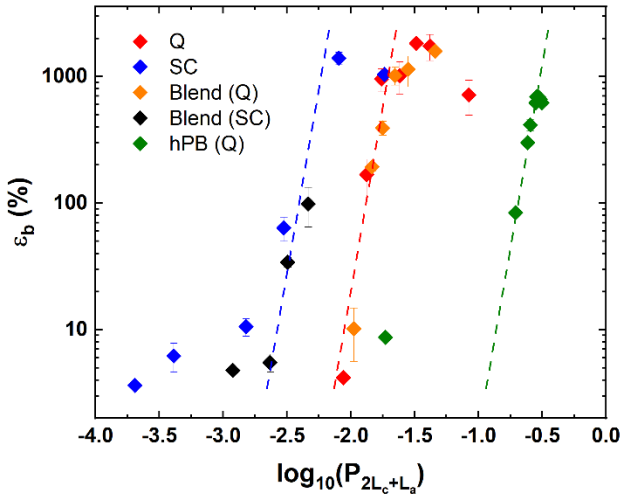

Figure 5. Breaking strain (ε_b) vs $\log_{10}(P_{2Lc+La})$ of individual LPEs and bimodal LPE blends with different thermal histories, and quenched hPBs, showing three different sharp brittle-to-ductile transitions. Dashed lines are guides to the eye. Note logarithmic ordinate scale for ε_b.

Figure 5 shows that while—as expected[9]—the ethyl branches in hPB do indeed greatly increase the TM content, hPB also *requires* substantially higher TM content to exceed the BDT and achieve ductility. As shown in Table 1, LPE37K(Q) is ductile (ε_b = 960%), while hPB42K, with a comparable M_n, is calculated to have an 11-fold higher TM content (P_{2Lc+La} = 0.19, where the maximum value of P allowed by Equation (1) is 1/3), but falls in the transition regime (ε_b = 84%). In other words, the increase in P which is achieved by incorporating short branches (thereby reducing d) is more than compensated for by the increase in P_{BDT} for hPB vs LPE crystallized under the same thermal history. Thus, Figure 5 unequivocally demonstrates that there is no universal threshold TM content dictating the BDT, but that in PE, P_{BDT} depends on thermal history and branch content.

The most obvious difference between the three classes of specimens in Figure 5 is their crystallinity. Figure 6 plots P_{BDT} vs ϕ_c for all specimens which fall in the "transition" regime

between brittle and ductile ($20 < \varepsilon_b < 200\%$), showing that P_{BDT} decreases exponentially with increasing ϕ_c. In these materials, ϕ_c and L_c are strongly correlated (see Table 1), so a comparable dependence is obtained when P_{BDT} is plotted against L_c (see Figure S26).

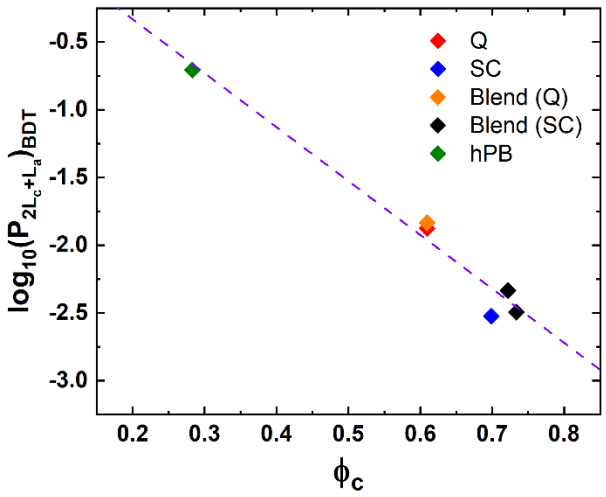

Figure 6. TM fraction at the BDT ($\log_{10}(P_{2Lc+La})_{BDT}$) vs volume fraction crystallinity (ϕ_c). Points correspond to the specimens that fail in "transition" mode, with $20 < \varepsilon_b < 200\%$, also indicated with footnote "a" in Table 1. Dashed line is a guide to the eye.

Stresses for yield vs brittle fracture. For PE to be ductile, stress transmitters (TMs and interlocking loops) must be able to transfer stress between crystal lamellae without significant pullout or chain rupture, such that yielding and fragmentation (either by crystallographic slip[63] or partial melting[64]) can initiate and propagate throughout the specimen. Thus, the BDT results from a competition between the brittle fracture stress (σ_b) and the yield stress (σ_y),[65-68] which represent the polymer's strength to resist rupture vs shear yielding of its crystals, respectively. If $\sigma_b < \sigma_y$, a polymer fractures in brittle fashion before it can yield.[65,68] Thus, ductility is favored by raising σ_b

or lowering σ_y—although to obtain a material which is both strong *and* ductile, the former is much preferred.

Over the broad range of ϕ_c and L_c explored here, σ_y is expected[34,69] to show some dependence on both quantities—and as noted above, ϕ_c and L_c are strongly correlated in these materials. Figure 7 shows the room-temperature σ_y for all materials in this study (values in Table 1) plotted against ϕ_c, demonstrating an excellent correlation. A comparable overall correlation is

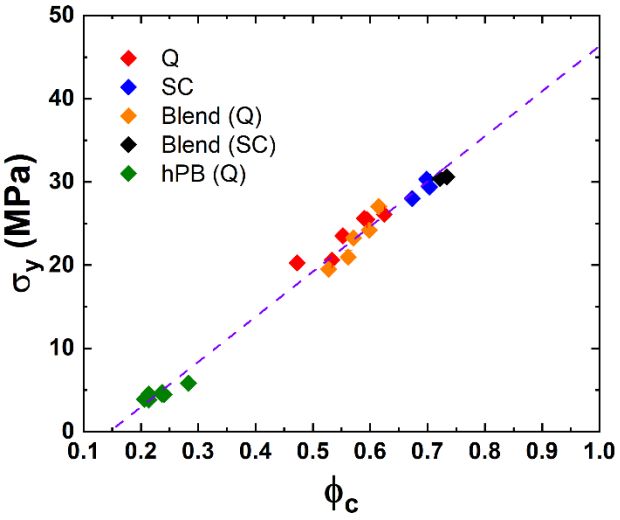

Figure 7. Yield stress (σ_y) vs volume fraction crystallinity (ϕ_c) for LPEs, LPE blends, and hPBs.

obtained for σ_y vs L_c (Supporting Information, Figure S27); the overall trend is that σ_y increases strongly with either ϕ_c or L_c. However, *within* either the LPE(SC) or LPE(Q) series, a steady decrease of σ_y with increasing M_n is observed (see Table 1), and as noted above, ϕ_c decreases substantially with M_n (Figure 3c) while L_c increases slightly (Figure 3b). Thus, a somewhat better correlation is obtained between σ_y and ϕ_c than between σ_y and L_c. In the following discussion, we

will refer to σ_y as being principally controlled by ϕ_c, while recognizing that L_c can also be an important quantity.

There is no direct influence of M on σ_y, since yielding involves processes at the length scale of the crystal stems, smaller than the whole-chain scale. The influence of M on σ_y is only indirect, through the effect of M on ϕ_c (Table 1 and Figure 3c), while ϕ_c is much more strongly modulated in LPE via thermal history (Q vs SC), or by the incorporation of branches/comonomer (as in hPB). Consequently, TM content has no influence on the value of σ_y (although as noted above, for σ_y to be measurable, the TM content must be sufficiently high that $\sigma_b > \sigma_y$).

On the other hand, a strong influence of TM content on the brittle fracture stress σ_b is expected. Indeed, measurement of σ_b at cryogenic temperatures, where the strengths of the crystal and amorphous phases are comparable, has been proposed as a method for measuring the content of TMs,[14] taking advantage of the fact that the ideal fracture strength of a solid is proportional to its modulus. Lu et al.[70] found that, for a range of PEs, quenching produced a higher cryogenic σ_b than slow-cooling, demonstrating that higher TM content in quenched specimens leads to higher σ_b. However, the situation at room temperature is rather different; since the modulus of the crystalline phase far exceeds that of the amorphous phase, σ_b is not solely a function of TM content, but depends on crystallinity as well. As an example, low-M waxes (paraffins) – which do not have any TMs, and thus always exhibit brittle failure – *do* have a nonzero strength, contributed by the crystallite framework (i.e., by ϕ_c). Measurements of the shear strength of paraffin waxes[71] show a clear correlation with the *n*-alkane (vs branched alkane) content, i.e., with ϕ_c. Adding TMs to the crystallite framework will further increase σ_b. However, the amount contributed by each TM to σ_b may depend on how "well-anchored" the TM is in the crystal. PE has a much-studied α

transition,[72] corresponding to a twist-shift motion of chain segments through the crystal;[73] the modulus of the amorphous phase can drop by an order of magnitude on passing through this transition.[54,72] The peak α transition temperature, T_α, decreases as the average crystal thickness L_c decreases;[74] as T_α approaches, and eventually drops below, the test temperature, the "anchoring" strength of the TM in the crystal is reduced, such that chain relaxation and even pullout become possible, effectively decreasing the contribution each TM makes to σ_b.

This idea is illustrated in Figure 8, which sketches σ_y and σ_b as functions of TM content, for three values of ϕ_c, corresponding conceptually to the three distinct classes of materials in Figure 5: LPE(SC), LPE(Q), and hPB (neglecting the modest variation of ϕ_c with M within each class). Since σ_y depends only on ϕ_c and not on TM content, σ_y is a horizontal line for each class, with σ_y(SC) > σ_y(Q) > σ_y(hPB). For the brittle fracture stress, at zero TM content, σ_b is entirely contributed by the crystallite framework (σ_{b0}), and like σ_y, σ_{b0} increases with ϕ_c. TMs make an additional contribution to σ_b, but with a slope related to the value of T_α relative to room temperature, which is correlated with the average crystal thickness L_c. For each case, the BDT occurs when the solid line (σ_y) and dashed line (σ_b) intersect. The depiction in Figure 8 is necessarily schematic, as neither the functional dependence of σ_{b0} on ϕ_c, nor the slopes of the dashed lines (corresponding to the TM contributions) are known. However, this schematic provides a qualitative framework for understanding the variation in P_{BDT}, and the BDT itself, as resulting from the subtle interplay between σ_b (a function of ϕ_c, TM content, and the strengths of the TMs as reflected in the slopes of the dashed lines in Figure 8) and σ_y (a function of ϕ_c only), and rationalizes the counterintuitive result that the BDT does not occur at a fixed value of P_{BDT}.

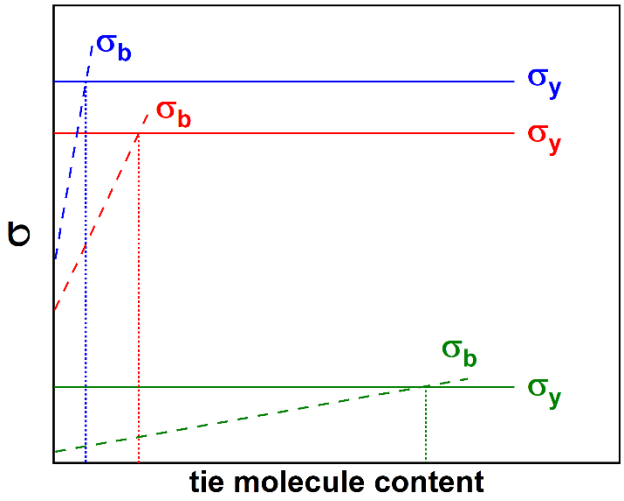

Figure 8. Schematic variation of σ_b (dashed lines) and σ_y (solid lines) with TM content, for polymers of high (blue), medium (red), and low (green) ϕ_c, qualitatively corresponding to LPE(SC), LPE(Q), and hPB, respectively. The dotted vertical lines correspond to the TM contents at the BDT (P_{BDT}), i.e., where $\sigma_b = \sigma_y$ for each of the three cases.

CONCLUSIONS

For a fixed thermal treatment or branch content, increasing M favors ductility in PE; in low-dispersity polymers, the BDT occurs over a relatively narrow range in M_n. However, the BDT does not occur at a universal TM fraction (P) across the series of thermal treatments and branch contents; rather, P_{BDT} increases strongly as ϕ_c decreases, by ≈50× between the LPE(SC) and hPB materials. This is most evident in comparing quenched samples of hPB and LPE; although d is ≈2× lower for hPB vs LPE, M_{BDT} is ≈1.5× *higher*. Thus, some molecular alterations made with the aim of increasing ductility (e.g., adding ethyl branches to reduce d at fixed M) actually favor brittle fracture instead. This behavior results from the fact that the BDT reflects the competition between brittle fracture (at a stress σ_b) and crystal yielding (at a stress σ_y); TMs raise σ_b but do not

influence σ_y, which is governed by crystallinity. In other words, M_{BDT} reflects not only the TM content, but also the crystallinity (both through σ_y, and through the contribution σ_{b0} made by the crystallite framework to σ_b). For the particular case of PE, the magnitude of the TM contribution to σ_b may depend significantly on the average crystal thickness, through the temperature of the PE α transition relative to the test temperature; the relative values of these two temperatures substantially influence the strength of the amorphous layer in PE. Future work will investigate whether this dependence is reduced or eliminated in polymers which do not show significant motion of the crystalline stems at room temperature, even in thin crystals.

ASSOCIATED CONTENT

Supporting Information

Molecular weight distribution curves; pictures of representative tensile specimens after failure; hPB crystallinity determined from density; stress-strain curves for all materials; SAXS patterns for all materials; d vs $\sqrt{M_n}$ for LPE); plots of ε_b, $\log_{10}(P_{2Lc+La})$, and σ_y vs alternative correlating quantities.

Corresponding Author

*Tel +1 609 258 4691; fax +1 609 258 0211; e-mail register@princeton.edu

Notes

The authors declare no competing financial interest.

Acknowledgements

This research was generously supported by the National Science Foundation, Polymers Program (DMR-2002991). The authors gratefully acknowledge Dr. William D. Mulhearn for the synthesis of hPB49K and hPB82K while at Princeton University.

REFERENCES

(1) Séguéla, R. Critical Review of the Molecular Topology of Semicrystalline Polymers: The Origin and Assessment of Intercrystalline Tie Molecules and Chain Entanglements. *J. Polym. Sci. Part B Polym. Phys.* **2005**, *43*, 1729–1748.

(2) Nitta, K. H.; Takayanagi, M. Role of Tie Molecules in the Yielding Deformation of Isotactic Polypropylene. *J. Polym. Sci. Part B Polym. Phys.* **1999**, *37*, 357–368.

(3) Men, Y.; Rieger, J.; Strobl, G. Role of the Entangled Amorphous Network in Tensile Deformation of Semicrystalline Polymers. *Phys. Rev. Lett.* **2003**, *91*, 095502.

(4) Patel, R. M.; Sehanobish, K.; Jain, P.; Chum, S. P.; Knight, G. W. Theoretical Prediction of Tie-Chain Concentration and Its Characterization Using Postyield Response. *J. Appl. Polym. Sci.* **1996**, *60*, 749–758.

(5) Kurelec, L.; Teeuwen, M.; Schoffeleers, H.; Deblieck, R. Strain Hardening Modulus as a Measure of Environmental Stress Crack Resistance of High Density Polyethylene. *Polymer* **2005**, *46*, 6369–6379.

(6) Mukherjee, P.; Ghosh, A.; Spegazzini, N.; Lamborn, M. J.; Monwar, M. M.; DesLauriers, P. J.; Bhargava, R. Relating Post-Yield Mechanical Behavior in Polyethylenes to Spatially Varying Molecular Deformation Using Infrared Spectroscopic Imaging: Homopolymers. *Macromolecules* **2018**, *51*, 3836–3844.

(7) Lustiger, A.; Markham, R. L. Importance of Tie Molecules in Preventing Polyethylene Fracture under Long-Term Loading Conditions. *Polymer* **1983**, *24*, 1647–1654.

(8) Huang, Y.-L.; Brown, N. The Effect of Molecular Weight on Slow Crack Growth in Linear

Polyethylene Homopolymers. *J. Mater. Sci.* **1988**, *23*, 3648–3655.

(9) Huang, Y.-L.; Brown, N. Dependence of Slow Crack Growth in Polyethylene on Butyl Branch Density: Morphology and Theory. *J. Polym. Sci. Part B Polym. Phys.* **1991**, *29*, 129–137.

(10) Brown, N.; Lu, X.; Huang, Y.-L.; Qian, R. Slow Crack Growth in Polyethylene - a Review. *Makromol. Chem. Macromol. Symp.* **1991**, *41*, 55–67.

(11) Brown, N.; Lu, X. A Fundamental Theory for Slow Crack Growth in Polyethylene. *Polymer* **1995**, *36*, 543–548.

(12) Keith, H. D.; Padden, F. J.; Vadimsky, R. G. Intercrystalline Links in Polyethylene Crystallized from the Melt. *J. Polym. Sci. Part A-2 Polym. Phys.* **1966**, *4*, 267–281.

(13) Keith, H. D.; Padden, F. J.; Vadimsky, R. G. Intercrystalline Links: Critical Evaluation. *J. Appl. Phys.* **1971**, *42*, 4585–4592.

(14) Brown, N.; Ward, I. M. The Influence of Morphology and Molecular Weight on Ductile-Brittle Transitions in Linear Polyethylene. *J. Mater. Sci.* **1983**, *18*, 1405–1420.

(15) Lustiger, A.; Ishikawa, N. An Analytical Technique for Measuring Relative Tie-molecule Concentration in Polyethylene. *J. Polym. Sci. Part B Polym. Phys.* **1991**, *29*, 1047–1055.

(16) McDermott, A. G.; DesLauriers, P. J.; Fodor, J. S.; Jones, R. L.; Snyder, C. R. Measuring Tie Chains and Trapped Entanglements in Semicrystalline Polymers. *Macromolecules* **2020**, *53*, 5614–5626.

(17) Stamm, M.; Fischer, E. W.; Dettenmaier, M.; Convert, P. Chain Conformation in the Crystalline State by Means of Neutron Scattering Methods. *Faraday Discuss. Chem. Soc.*

1979, *68*, 263–278.

(18) Dettenmaier, M.; Fischer, E. W.; Stamm, M. Calculation of Small-Angle Neutron Scattering by Macromolecules in the Semicrystalline State. *Colloid Polym. Sci.* **1980**, *258*, 343–349.

(19) Schelten, J.; Ballard, D. G. H.; Wignall, G. D.; Longman, G.; Schmatz, W. Small-Angle Neutron Scattering Studies of Molten and Crystalline Polyethylene. *Polymer* **1976**, *17*, 751–757.

(20) Schelten, J.; Wignall, G. D.; Ballard, D. G. H.; Longman, G. W. Small-Angle Neutron Scattering Studies of Molecular Clustering in Mixtures of Polyethylene and Deuterated Polyethylene. *Polymer* **1977**, *18*, 1111–1120.

(21) Tanzer, J. D.; Bartels, C. R.; Crist, B.; Graessley, W. W. Dimensions of Polymer Chains in the Semicrystalline Solid State. *Macromolecules* **1984**, *17*, 2708–2714.

(22) Ballard, D. G. H.; Cheshire, P.; Longman, G. W.; Schelten, J. Small-Angle Neutron Scattering Studies of Isotropic Polypropylene. *Polymer* **1978**, *19*, 379–385.

(23) Li, S.; Register, R. A. Crystallization in Copolymers. In *Handbook of Polymer Crystallization*; Piorkowska, E., Rutledge, G. C., Eds.; John Wiley & Sons, Inc.: Hoboken, NJ, USA, 2013; pp 327–346.

(24) DesLauriers, P. J.; McDaniel, M. P.; Rohlfing, D. C.; Krishnaswamy, R. K.; Secora, S. J.; Benham, E. A.; Maeger, P. L.; Wolfe, A. R.; Sukhadia, A. M.; Beaulieu, B. B. A Comparative Study of Multimodal vs. Bimodal Polyethylene Pipe Resins for PE-100 Applications. *Polym. Eng. Sci.* **2005**, *45*, 1203–1213.

(25) Krishnaswamy, R. K.; Yang, Q.; Fernandez-Ballester, L.; Kornfield, J. A. Effect of the

Distribution of Short-Chain Branches on Crystallization Kinetics and Mechanical Properties of High-Density Polyethylene. *Macromolecules* **2008**, *41*, 1693–1704.

(26) Adib, A.; Domínguez, C.; Rodríguez, J.; Martín, C.; García, R. A. The Effect of Microstructure on the Slow Crack Growth Resistance in Polyethylene Resins. *Polym. Eng. Sci.* **2015**, *55*, 1018–1023.

(27) DesLauriers, P. J.; Rohlfing, D. C. Estimating Slow Crack Growth Performance of Polyethylene Resins from Primary Structures Such as Molecular Weight and Short Chain Branching. *Macromol. Symp.* **2009**, *282*, 136–149.

(28) Fodor, J. S.; DesLauriers, P. J.; Lamborn, M. J.; Hamim, S. U. Further Investigation of the Relationship between Polymer Structure and HDPE Post Yield Properties. *Polymer* **2019**, *180*, 121730.

(29) Tung, L. Tensile Properties of Fractionated High Density Polyethylenes. *SPE J.* **1958**, *14*, 25–28.

(30) Williamson, G. R.; Wright, B.; Haward, R. N. The Preparation and Properties of Fractions from High Density Polyethylenes. *J. Appl. Chem.* **1964**, *14*, 131–140.

(31) Kenyon, A. S.; Salyer, I. O.; Kurz, J. E.; Brown, D. R. Large-Scale Elution Fractionation of Polymers. *J. Polym. Sci. Part C Polym. Symp.* **1965**, *8*, 205–216.

(32) Fulmer, G. E.; Horowitz, R. H. Stress-Strain Properties of Narrow Molecular Weight Fractions of Linear Polyethylene. In *Proceedings of the VIIth International Congress on Rheology, Chalmers University of Technology, Gothenburg, Sweden, August 23 - August 27, 1976*; Swedish Society of Rheology: Gothenburg, Sweden, 1976; pp 624–625.

(33) Gol'dman, A. Y.; Shcherbak, V. V.; Andreyeva, I. N. Study of the Influence of Molecular Structure on the Durability of High Density Polyethylene Fractions. *Polym. Sci. U.S.S.R.* **1977**, *19*, 2953–2961.

(34) Kennedy, M. A.; Peacock, A. J.; Mandelkern, L. Tensile Properties of Crystalline Polymers: Linear Polyethylene. *Macromolecules* **1994**, *27*, 5297–5310.

(35) Mulhearn, W. D.; Register, R. A. Synthesis of Narrow-Distribution, High-Molecular-Weight ROMP Polycyclopentene via Suppression of Acyclic Metathesis Side Reactions. *ACS Macro Lett.* **2017**, *6*, 112–116.

(36) Burns, A. B.; Register, R. A. Thermoplastic Elastomers via Combined Crystallization and Vitrification from Homogeneous Melts. *Macromolecules* **2016**, *49*, 269–279.

(37) Trzaska, S. T.; Lee, L.-B. W.; Register, R. A. Synthesis of Narrow-Distribution "Perfect" Polyethylene and Its Block Copolymers by Polymerization of Cyclopentene. *Macromolecules* **2000**, *33*, 9215–9221.

(38) Rochefort, W. E.; Smith, G. G.; Rachapudy, H.; Raju, V. R.; Graessley, W. W. Properties of Amorphous and Crystallizable Hydrocarbon Polymers. II. Rheology of Linear and Star-Branched Polybutadiene. *J. Polym. Sci. Polym. Phys. Ed.* **1979**, *17*, 1197–1210.

(39) Tanzer, J. D. Chain Dimensions of Isotropic and Deformed Semi-Crystalline Polymers by Small-Angle Neutron Scattering, Ph.D. Thesis, Northwestern University, 1985.

(40) Cho, S. H.; Pelczer, I.; Register, R. A. Regularity of Deuteration in Linear Polyethylene Prepared by Saturation of Polycyclopentene over Homogeneous Catalysts. *Macromolecules* **2021**, *54*, 10300–10311.

(41) Xu, Z.; Hadjichristidis, N.; Carella, J. M.; Fetters, L. J. Characteristic Ratios of Atactic Poly(vinylethylene) and Poly(ethylethylene). *Macromolecules* **1983**, *16*, 925–929.

(42) Rosedale, J. H.; Bates, F. S. Heterogeneous Catalytic Hydrogenation of Poly(vinylethylene). *J. Am. Chem. Soc.* **1988**, *110*, 3542–3545.

(43) Rangarajan, P.; Register, R. A.; Fetters, L. J. Morphology of Semicrystalline Block Copolymers of Ethylene-(Ethylene-*alt*-propylene). *Macromolecules* **1993**, *26*, 4640–4645.

(44) Sebastian, J. M.; Register, R. A. Block Copolymer Molecular Weight Determination via Gel Permeation Chromatography: Choosing a Combining Rule. *J. Appl. Polym. Sci.* **2001**, *82*, 2056–2069.

(45) Mulhearn, W. D.; Register, R. A. Yield Stress Enhancement in Polyethylene-Glassy Diblock Copolymers. *Macromolecules* **2017**, *50*, 9666–9673.

(46) Mandelkern, L.; Smith, F. L.; Failla, M.; Kennedy, M. A.; Peacock, A. J. The Brittle-Ductile Transition in Linear Polyethylene. *J. Polym. Sci. B: Polym. Phys.* **1993**, *31*, 491-493.

(47) Lake, J. A. An Iterative Method of Slit-Correcting Small Angle X-Ray Data. *Acta Crystallogr.* **1967**, *23*, 191–194.

(48) Register, R. A.; Bell, T. R. Miscible Blends of Zinc-Neutralized Sulfonated Polystyrene and Poly(2,6-dimethyl 1,4-phenylene oxide). *J. Polym. Sci. Part B Polym. Phys.* **1992**, *30*, 569–575.

(49) Alexander, L. E. X-Ray Diffraction Methods in Polymer Science; John Wiley & Sons, Inc.: New York, NY, 1969; p 284.

(50) Wunderlich, B.; Cormier, C. M. Heat of Fusion of Polyethylene. *J. Polym. Sci. Part A-2*

Polym. Phys. **1967**, *5*, 987–988.

(51) Swan, P. R. Polyethylene Unit Cell Variations with Temperature. *J. Polym. Sci.* **1962**, *56*, 403–407.

(52) Allen, G.; Gee, G.; Wilson, G. J. Intermolecular Forces and Chain Flexibilities in Polymers: I. Internal Pressures and Cohesive Energy Densities of Simple Liquids. *Polymer* **1960**, *1*, 456–466.

(53) Tanzer, J. D.; Crist, B.; Graessley, W. W. Chain Dimensions in Plastically Deformed Semicrystalline Polymers. *J. Polym. Sci. Part B Polym. Phys.* **1989**, *27*, 859–874.

(54) Crist, B.; Fisher, C. J.; Howard, P. R. Mechanical Properties of Model Polyethylenes: Tensile Elastic Modulus and Yield Stress. *Macromolecules* **1989**, *22*, 1709–1718.

(55) Krigas, T. M.; Carella, J. M.; Struglinski, M. J.; Crist, B.; Graessley, W. W.; Schilling, F. C. Model Copolymers of Ethylene with Butene-1 Made by Hydrogenation of Polybutadiene: Chemical Composition and Selected Physical Properties. *J. Polym. Sci. Polym. Phys. Ed.* **1985**, *23*, 509–520.

(56) Fetters, L. J.; Lohse, D. J.; Richter, D.; Witten, T. A.; Zirkel, A. Connection between Polymer Molecular Weight, Density, Chain Dimensions, and Melt Viscoelastic Properties. *Macromolecules* **1994**, *27*, 4639–4647.

(57) Robelin-Souffaché, E.; Rault, J. Origin of the Long Period and Crystallinity in Quenched Semicrystalline Polymers. 1. *Macromolecules* **1989**, *22*, 3581–3594.

(58) Rault, J.; Robelin-Souffaché, E. Long Periods in Slow-cooled Linear and Branched Polyethylene: Part II. *J. Polym. Sci. Part B Polym. Phys.* **1989**, *27*, 1349–1373.

(59) Barham, P. J.; Chivers, R. A.; Keller, A.; Martinez-Salazar, J.; Organ, S. J. The Supercooling Dependence of the Initial Fold Length of Polyethylene Crystallized from the Melt: Unification of Melt and Solution Crystallization. *J. Mater. Sci.* **1985**, *20*, 1625–1630.

(60) Hoffman, J. D.; Miller, R. L. Kinetics of Crystallization from the Melt and Chain Folding in Polyethylene Fractions Revisited: Theory and Experiment. *Polymer* **1997**, *38*, 3151–3212.

(61) Yeh, J. T.; Runt, J. Fatigue Crack Propagation in High-Density Polyethylene. *J. Polym. Sci. Part B Polym. Phys.* **1991**, *29*, 371–388.

(62) Ranganathan, R.; Kumar, V.; Brayton, A. L.; Kröger, M.; Rutledge, G. C. Atomistic Modeling of Plastic Deformation in Semicrystalline Polyethylene: Role of Interphase Topology, Entanglements, and Chain Dynamics. *Macromolecules* **2020**, *53*, 4605–4617.

(63) Young, R. J. A Dislocation Model for Yield in Polyethylene. *Philos. Mag.* **1974**, *30*, 85–94.

(64) Yoon, D. Y.; Flory, P. J. Molecular Morphology in Semicrystalline Polymers. *Faraday Discuss. Chem. Soc.* **1979**, *68*, 288–296.

(65) Orowan, E. Fracture and Strength of Solids. *Rep. Prog. Phys.* **1949**, *12*, 185–232.

(66) Perkins, W. G. Polymer Toughness and Impact Resistance. *Polym. Eng. Sci.* **1999**, *39*, 2445–2460.

(67) Sanner, M. A.; Haralur, G.; May, A. Effect of Molecular Weight on Brittle-to-Ductile Transition Temperature of Polyetherimide. *J. Appl. Polym. Sci.* **2004**, *92*, 1666–1671.

(68) Ward, I. M.; Sweeney, J. *Mechanical Properties of Solid Polymers*; John Wiley & Sons, Ltd: Chichester, UK, 2012.

(69) Kazmierczak, T.; Galeski, A.; Argon, A. S. Plastic Deformation of Polyethylene Crystals as a Function of Crystal Thickness and Compression Rate. *Polymer* **2005**, *46*, 8926–8936.

(70) Lu, X.; Qian, R.; Brown, N. The Effect of Crystallinity on Fracture and Yielding of Polyethylenes. *Polymer* **1995**, *36*, 4239–4244.

(71) Abubakarova, A. S.; Khadisova, Z. T.; Aleksandrova, E. A.; Krasavtsev, B. E. Study of Structural-Mechanical Properties of Paraffin-Containing Petroleum Products. *Chem. Technol. Fuels Oils* **2014**, *50*, 149–155.

(72) Boyd, R. H. Relaxation Processes in Crystalline Polymers: Experimental Behaviour - a Review. *Polymer* **1985**, *26*, 323–347.

(73) Boyd, R. H. Relaxation Processes in Crystalline Polymers: Molecular Interpretation - a Review. *Polymer* **1985**, *26*, 1123–1133.

(74) Khanna, Y. P.; Turi, E. A.; Taylor, T. J.; Vickroy, V. V.; Abbott, R. F. Dynamic Mechanical Relaxations in Polyethylene. *Macromolecules* **1985**, *18*, 1302–1309.